Temperature-dependent properties of 147- and 309-atom iron-gold nanoclusters

Rafael I. González
Facultad de Física, Pontificia Universidad Católica de Chile, Casilla 306, Santiago, Chile

G. García, R. Ramírez, and Miguel Kiwi
Facultad de Física, Pontificia Universidad Católica de Chile, Casilla 306, Santiago, Chile and Centro para el Desarrollo de la Nanociencia y la Nanotecnología, CEDENNA, Avenida Ecuador 3493, Santiago, Chile

J. A. Valdivia
Departamento de Física, Facultad de Ciencias, Universidad de Chile, Casilla 653, Santiago, Chile and Centro para el Desarrollo de la Nanociencia y la Nanotecnología, CEDENNA, Avenida Ecuador 3493, Santiago, Chile

Talat S. Rahman
Department of Physics, University of Central Florida, P.O. Box 162385, Orlando, Florida 32816-2385, USA
(Received 20 August 2010; published 14 April 2011)

The properties of several Au_N and $Au_{N-x}Fe_x$ nanoclusters are obtained by means of classical molecular dynamics calculations. In particular we study the configurations Au_{147}, $Au_{134}Fe_{13}$, Au_{309}, and $Au_{254}Fe_{55}$, which correspond to icosahedral magic numbers, for both the gold and the iron. We investigate the melting and freezing processes, atomic diffusion, hardness, vibration spectra, and specific heat of these nanoclusters. All the data obtained point toward the stability of the $Au_{N-x}Fe_x$ system, with the gold atoms on the outside of the iron core.

DOI: 10.1103/PhysRevB.83.155425 PACS number(s): 36.40.Ei, 36.40.Qv, 63.22.Kn

I. INTRODUCTION

The properties of nanoparticles have received significant attention for quite some time. Nanosized metal colloids were already investigated in 1857 by Faraday.[1] Some 30 years ago Buffat and Borel[2] established experimentally the size-dependent melting of gold clusters in the range of 3–30 nm in diameter. However, the boom of the field encompasses mostly the last two decades. A milestone was set by Haruta[3] in 1997 with a systematic study of the properties of nanoscale materials and his finding of enhanced reactivity of gold nanoparticles. Actually, nanosized particles display remarkable catalytic,[4,5] electronic,[6,7] magnetic,[8] optical,[9] and mechanical[10] properties, which depart significantly from bulk behavior. These novel properties have also triggered theoretical evaluation of the stability and structural evolution of the nanoparticles as a function of temperature.[11–14]

The unusual properties of gold nanoparticles[3–5] have prompted experimental and theoretical investigations aimed at discovering novel properties when Au alloys with other transition metals.[15] An interesting combination is that of Au and Fe, which although immiscible in the bulk, forms Au-Fe layered films whose properties (magnetic anisotropy, enhanced Curie temperature, intense interband absorption peak, structure dependent absorption characteristics, etc.) make them ripe for optical and magneto-optical applications.[16–18] Recently, Au-Fe nanoparticles (50-50 composition) synthesized by Roldan's group were found to be remarkably stable[19] on titania as substrate, while their structure depended on the annealing temperature. Although the exact nature of the structure is not known, these detailed STM and x-ray photoelectron spectroscopy (XPS) measurements predict it to vary from phase segregated, to homogeneous alloy, to core-shell (Au at the surface). The 80% Au–20% Fe nanoalloy, on the other hand, appears to be the most stable vis á vis geometrical disorder.[20] Questions have been raised about the propensity of Au atoms to diffuse to the surface as a function of composition and temperature.

The interest in Au-Fe nanoparticles is, of course, not new. In 1999, Koga *et al.*[21] prepared 2–10 nm Au-Fe particles and found the structure, as measured by high-resolution transmission electron microscopy (HRTEM), to be icosahedral and the morphology to be retained even after annealing. Since the bulk Au-11%-Fe alloy is known to phase segregate into Au and α-Fe at 710 K,[22] the thermally stable structure of the nanoalloy is intriguing. Questions have been raised about whether the stabilization of the icosahedral structure is a result of electronic effects or due to strain relief arising from the smaller Fe atoms (the Fe atom is about 14% smaller than Au).[21] The coating of Fe nanoparticles by Au has also been suggested as a way to protect the Fe from oxidation while at the same time retaining its magnetic property. The obvious question is whether the nanoparticles with magnetic core and Au shell retain their magnetic properties. Paulus *et al.*[23] have suggested that the Fe-Au nanoparticles do not retain their core-shell structure, but rather undergo mixing. On the other hand, TEM and HREM measurements of nanoparticles from a two-stage growth process using inverse micelles, by Zhou *et al.*,[24] confirm the Fe-core/Au-shell structure but with magnetic moments similar to bulk Fe.

Motivated by the above, and keeping in mind that the iron core offers the possibility of magnetic steering of the nanoclusters with significant biomedical applications, we have carried out molecular dynamics simulations of the temperature-dependent structure and dynamics of a set of Au-Fe nanoalloys. In particular, we investigate the properties of magic number sized clusters of 147 and 309 atoms. For the time being we limited our attention to four closed-shell systems: Au_{147}, $Au_{134}Fe_{13}$, Au_{309}, and $Au_{254}Fe_{55}$. By means of

 © 2011 American Physical Society

classical molecular dynamics (MD) simulations we obtained information on the melting and freezing process, atomic diffusion, hardness, vibration spectrum, and specific heat of these nanoparticles.

This paper is organized as follows: After this introduction the MD method is described in Sec. II, the melting dynamics in Sec. III, the atomic diffusion in Sec. IV, the cluster hardness in Sec. V, and the vibration spectra, density of states, and specific heat in Sec. VI. Finally, Sec. VII closes the paper summarizing our findings and drawing conclusions.

II. MOLECULAR DYNAMICS SIMULATION

The properties and behavior of Au-Fe clusters, over a wide range of temperatures, were simulated by means classical molecular dynamics using a code by Ercolessi,[25,26] which we modified to accept Finnis-Sinclair type potentials. The equations of motion were integrated with a fifth-order predictor corrector algorithm using a time step of 1 femtosecond. Temperature was controlled by means of a Nosé-Hoover thermostat.

For the Au-Au and Fe-Fe interactions we have used Finnis-Sinclair (FS) potentials[27] as modified by Dai *et al.*, both for bcc and fcc lattices,[28] which improves agreement with experiment. This is achieved by adding a sixth-degree term to the pair potential and a quartic term to the density function. To determine the Au-Fe interaction we first constructed an ideal Au-Fe "bcc" lattice, from which we obtain the potential energy through a DFT calculation using VASP,[29–31] for several values of the lattice constant. In these calculations projector augmented wave (PAW-GGA) pseudopotentials, for both Au and Fe, were used with an energy cutoff of 230 eV. For the exchange-correlation functional we used the spin-polarized generalized conjugate gradient approximation. Only the Γ point was evaluated in the Brillouin zone integration with a Monkhorst-Pack k-point mesh of 56 k points.

These energies were then used to fit the Au-Fe FS potential as modified by Dai. In this version of the FS formalism the total potential energy is given by

$$U_{\text{tot}} = \frac{1}{2}\sum_{ij} V(r_{ij}) - \sum_{i} f(\rho_i)\,, \tag{1}$$

where

$$V(r) = \begin{cases} (r-c)^2(c_0 + c_1 r + c_2 r^2 + c_3 r^3 + c_4 r^4)\,, & r \leqslant c\,, \\ 0\,, & r > c\,, \end{cases} \tag{2}$$

$$f(\rho_i) = \sqrt{\rho_i}\,, \tag{3}$$

$$\rho_i = \sum_{j\neq i} A^2 \phi(r_{ij})\,, \tag{4}$$

$$\phi(r) = \begin{cases} (r-d)^2 + B^2(r-d)^4\,, & r \leqslant d\,, \\ 0\,, & r > d\,. \end{cases} \tag{5}$$

The values of the parameters we used in our MD simulations are given in Table I. We also checked that the geometric mean of these Au and Fe parameters are in excellent agreement with the fitted Finnis-Sinclair Au-Fe parameters.

TABLE I. Finnis-Sinclair potential (Dai modified) parameters (Refs. 27 and 28).

	Au	Fe	Au-Fe
A (eV/Å)	0.0137025	0.931312	0
d (Å)	4.41	4.05	0
c (Å)	4.76	2.96	4.23699
c_0 (eV/Å^2)	44.96858	26.27034	35.4272
c_1 (eV/Å^3)	−55.12826	−24.40109	−40.0155
c_2 (eV/Å^4)	25.84657	6.957871	16.2309
c_3 (eV/Å^5)	−5.44922	−0.303077	−2.6723
c_4 (eV/Å^6)	0.43266	−0.085092	0.130014
B (Å^{-2})	−53.9630	0	0

III. THE HEATING AND COOLING PROCESSES

We studied the behavior of both pure gold and iron-filled gold clusters. In particular, we investigated two different sized systems: (i) the 147-atom clusters, Au_{147} and $Au_{134}Fe_{13}$, and (ii) the 309-atom ones, Au_{309} and $Au_{254}Fe_{55}$. They correspond to closed shells (magic numbers) of the respective gold clusters and also of the interior iron core.

We evaluated the total energy as a function of temperature T for all the above-mentioned clusters, from 20 K up to well above the melting temperature (see Fig. 1). Note that our interest here is not the exact determination of the cluster melting temperature, for which much more accuracy is needed in the interatomic potential and some modifications of the calculational procedure. Rather, we are interested in comparing the heating process for the pure gold and the corresponding alloy nanoparticle, and on the relative melting temperature variation with cluster size.[32] With this objective T was increased in 20 K steps during the simulations and the system was relaxed at every T step for 0.5 ns (i.e., half a million MD steps). Thereafter T was decreased at the same pace, down to 20 K. We observe a completely different behavior of the pure gold clusters as compared with the Au-Fe ones, as illustrated in Fig. 1. For pure Au_{147} and Au_{309} we distinguish three regions: (i) The first corresponds to heating until the vicinity of the melting point is reached from below. A linear energy vs temperature relation holds, while the clusters roughly maintain their icosahedral shape.[21] (ii) The second region corresponds to the vicinity of the fusion point where we observe a hysteresis loop, reminiscent of a first-order phase transition. The energy drop during heating for our binary nanoclusters is just caused by the choice of the initial structure, which does not correspond to an energy minimum, but rather to a higher energy high-symmetry configuration. Thus, we see the difference between the increasing (black circles) and decreasing (red crosses) temperature branches, as better displayed in the inset on the left panel of Fig. 1. (iii) The third region corresponds to a liquid gold phase, characterized by a large atomic mobility, and will be discussed in detail in Sec. IV below.

$Au_{134}Fe_{13}$ and $Au_{254}Fe_{55}$ display a quite different behavior, when compared to the pure gold structures. The green squares

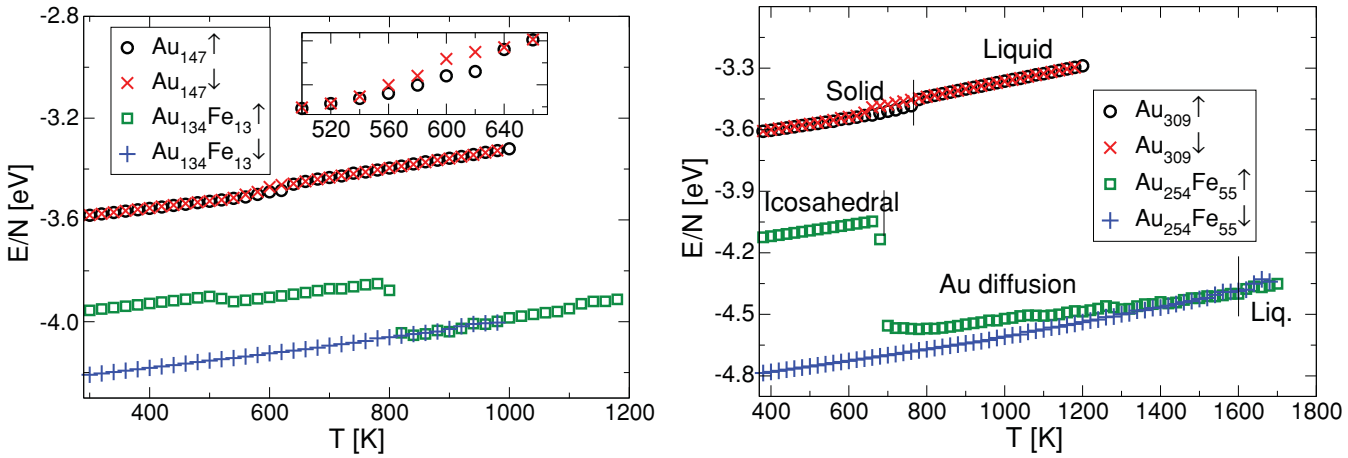

FIG. 1. (Color online) Energy versus temperature for Au_{147} and $Au_{134}Fe_{13}$ (left panel), and Au_{309} and $Au_{254}Fe_{55}$ (right panel) clusters. The black open circles describe the heating (↑) and the red crosses the cooling (↓) process of pure icosahedric 147- and 309-atom gold clusters. For the Au_{147} cluster a hysteresis loop is observed around 600 K (see inset). The green squares illustrate the heating process of the $Au_{134}Fe_{13}$ and $Au_{254}Fe_{55}$ clusters, which show a sharp transition around 800 K and 700 K, respectively, as the clusters overcome the kinetic barrier. The blue + symbols describe the cooling from the liquid, as the clusters adopt a lower energy configuration than the original one.

in Fig. 1 illustrate the heating process of the clusters. A sharp transition is observed as the clusters overcome the kinetic barrier,[32] suffer a morphological transformation, and recrystallize, settling into a lower energy configuration. Above these temperatures (≈800 and ≈700 K for $Au_{134}Fe_{13}$ and $Au_{254}Fe_{55}$, respectively) there is a large mobility, mainly of the gold atoms on the cluster "surface," as the system works its way to a lower energy configuration. However, when the temperature is reduced back to 20 K (blue + symbols in Fig. 1) the energy evolves smoothly, as the system adopts a lower energy low-symmetry configuration, different from the original icosahedron, as illustrated in Fig. 2 for $Au_{134}Fe_{13}$, which implies that the icosahedral configuration we adopted initially is not the minimal energy one, but corresponds to a higher energy metastable structure. If the system undergoes a new temperature cycle this lower energy configuration is preserved.

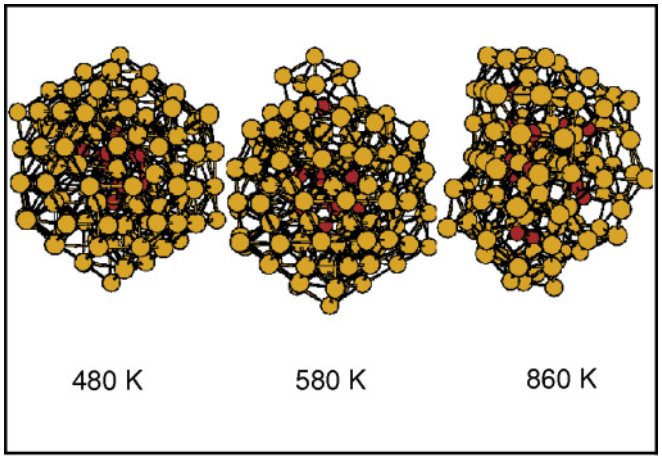

FIG. 2. (Color online) Configuration of $Au_{134}Fe_{13}$ at three different temperatures.

It is worth mentioning that our results follow the experimental and theoretical trends established by previous authors. In fact, Schmidt *et al*. determined experimentally a 33% reduction of the melting temperature of 192-atom sodium clusters.[33,34] On the other hand Mottet and Goniakowski[32] modeled the melting and freezing processes of Pd nanoclusters on a MgO substrate and observed both a reduction of the Pd clusters' melting and freezing temperatures and caloric curves quite similar to Fig. 1. That is, the Au-Fe alloying we investigate yields results that bear some relation with supporting the clusters on a substrate, which also incorporates the interaction of different chemical elements.

Actually, the melting of bimetallic nanoparticles continues to be the subject of a number of theoretical studies, most of which have relied on molecular dynamics simulation.[11–14] The subject is particularly interesting when the cluster shell is of a metal of lower bulk melting temperature than the core, since there is the expectation that the surface of the nanoparticle will melt before the core, and that the molten shell may protect the functionalities of the core. We note here a few findings along these lines that already exist in the literature.

VanHoof and Hou[11] used Monte Carlo and static molecular methods to show that for Ag-Co core-shell nanoparticles, the Ag shell induces an expansion of the Co core, while the Co core induces an average contraction of the Ag lattice. Moreover, the Co cores melt at temperatures lower than for bulk Co and this temperature is not sensitive to the thickness of the Ag shell. The melting temperature of the Ag shell is significantly lower than of the Co core, suggesting a solid core and a liquid shell for these nanoparticles. For core-shell Ag-Co (and Ag-Ni) nanoparticles, containing 45 and 127 atoms, Kuntova *et al*.[12] carried out MD simulations to find that the Ag shell indeed melts first and that there is a substantial difference in the melting temperature of the core and the shell. In the case of Ag-Pd bimetallic clusters,[13] the melting temperature was found to be lower than that of the bulk state and to rise as the

cluster size and the Pd composition increase. The melting of the cluster was found to start at the surface layer.

Very recent work of Li *et al.*[14] for Co, Co-Cu, and Co-Ni clusters find irregular melting induced by Cu atomic segregation and that the melting temperature can be controlled by doping heteroatoms with different surface energies.

The exact definition of melting temperature for these small nanoparticles is, however, ambiguous, something that we have also encountered in our studies and have thus refrained from placing emphasis on. Instead, we have concentrated on other temperature-dependent characteristics of the nanoparticles that are more uniquely defined.

IV. DIFFUSION

In this section we discuss the motion of the atoms, as the clusters are subject to varying temperatures. The diffusion of the atoms in the cluster is strongly dependent on temperature. In Fig. 3 we display the mean square displacement (MSD), defined as $\langle(\vec{r}-\vec{r}_0)^2\rangle$, where $\vec{r}_0$ are the original positions of the atoms and $\vec{r}$ the coordinates they adopt as time evolves.

It is quite apparent that the MSD is severely reduced when Au is replaced by Fe in the interior of the clusters, as indicated by the tenfold difference in y-axis scale of the upper panel of Fig. 3, in relation to the middle and lower ones. That is, in a pure atom cluster the atomic diffusion is much larger than in binary structures. However, above the melting temperature $\langle(r-r_0)^2\rangle$ initially always grows linearly with time, which is characteristic of a liquid phase, but it reaches a saturation value due to the finite size of the system.

As already mentioned, for $Au_{134}Fe_{13}$ there is a linear evolution of the energy for temperatures up to 500 K (see Fig. 1). Above this temperature at least one of the Fe atoms moves close to the cluster surface, but it is encapsulated by the Au atoms (see middle picture of Fig. 2). As the temperature increases above 780 K, we observe a marked energy decrease and the cluster becomes amorphous. However, no Fe atom reaches the surface, in spite of the fact that the mobility of Au and Fe are quite different. From 800 K to 1100 K one observes Au self-diffusion and an increase of its mean square displacement $\langle(r-r_0)^2\rangle$, as illustrated by Fig. 3. Above 1100 K the $\langle(r-r_0)^2\rangle$ both for Fe and Au grows linearly with time. As far as the diffusion dynamics as described by MSD is concerned, the behavior of the 309-atom clusters differ only quantitatively from the 147-atom ones described above, as can be verified by inspection of Fig. 3.

Figure 4 illustrates, in a different fashion, the atomic diffusion near the melting temperature for Au_{147} and Au_{309} clusters. The abscissa corresponds to the average distance to the center of mass of each atom in the cluster; this distance is averaged over the 0.5 ns at every temperature step. The y axis is the speed at which the atoms travel, along an arbitrary path, to reach the position $\vec{r}$ at the end of that particular temperature step. An atom is defined to move if its displacement away from its instantaneous position is larger than one-half of the average interatomic distance.

In the left panel of Fig. 4 we illustrate the atomic motion for Au_{147}. We observe that below 540 K the atoms barely move. As T reaches 580 K the atoms on the outermost shell begin to diffuse, while atoms closer to the cluster core remain almost fixed. This becomes more evident as the temperature reaches 620 K, when most atoms are changing positions but still four atomic shells can be clearly distinguished, corresponding to the magic numbers 1, 13, 55, and 147. Finally, at 640 K all the atoms participate in the diffusion dynamics. This temperature value is the same at which the energy of the system has a sharp kink in the E/N vs T plot shown in Fig. 1, as displayed in detail in the inset of the left panel of the same figure. A similar process occurs for Au_{309}, as can be seen in the right panel of Fig. 4, but for slightly higher temperatures.

For the binary clusters $Au_{134}Fe_{13}$ and $Au_{254}Fe_{55}$ we choose a slightly different way of illustrating the MD results, due to the fact that they completely loose the icosahedral structure, adopting a rather irregular shape, which makes the definition of atomic shells rather ambiguous. Thus, in Fig. 5 we adopt the average Au-Fe coordination number as our independent variable. The speed of the Fe atoms is marked by (red) crosses, while Au is denoted by (black) open circles. The sharp contrast

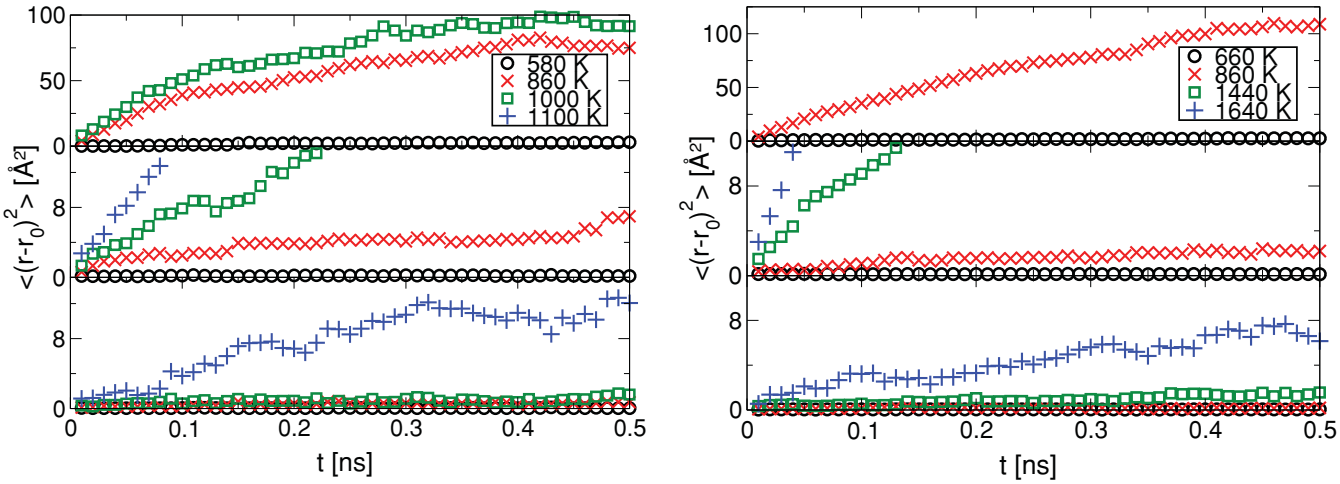

FIG. 3. (Color online) Mean square displacement of the atoms of 147 (left panel) and 309 (right panel) atom clusters as a function of time, for different temperature values from 580 to 1640 K. The upper panels correspond to Au_{147} (left) and Au_{309} (right). The middle and lower ones illustrate the mean square displacement of Au and Fe atoms, respectively, of $Au_{134}Fe_{13}$ (left) and $Au_{254}Fe_{55}$ clusters.

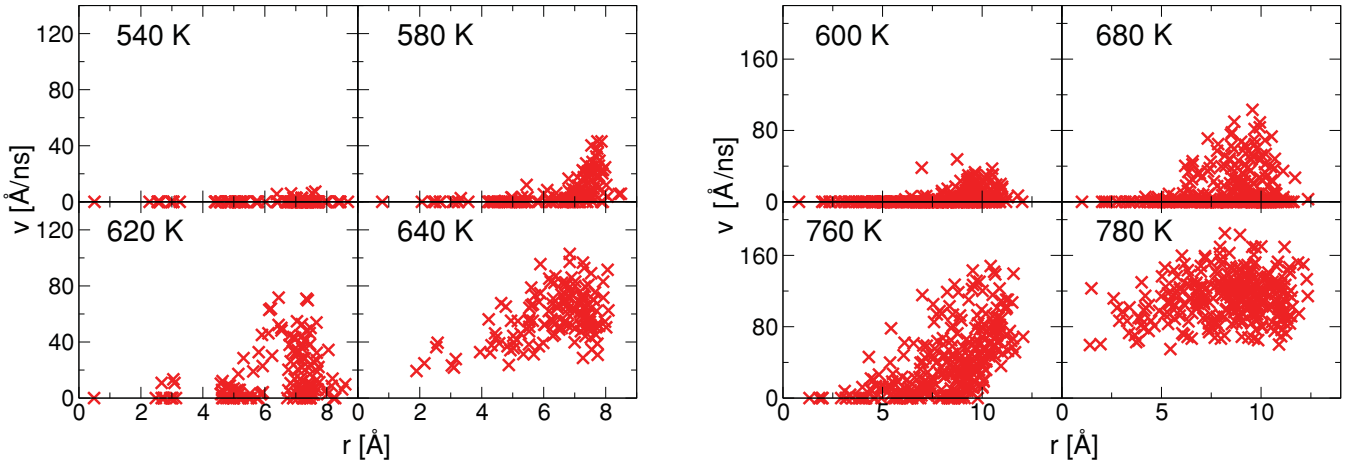

FIG. 4. (Color online) Atomic displacement speed versus center-of-mass distance for Au_{147} (left panel) and Au_{309} (right panel) clusters.

between the large gold atomic diffusion and the much smaller Fe one is quite apparent, both for the 147- and the 309-atom clusters. This underlines the fact that iron is contained in the inside by the outer gold shells, a feature which has relevant implications for practical uses.

V. HARDNESS

According to electron microscope observations by Saha *et al.*[21] the icosahedral structure of Au-Fe nanoparticles is preserved up to around 700 K, with no diffusion of Fe atoms toward the cluster surface. This is in agreement with our calculations (see the right panel of Fig. 1). In order to assess the importance of the Fe atoms on the stability of the cluster we computed the variation of the total potential energy versus small changes of the distance of every atom to the center of mass of the cluster (radial rescaling). The results are shown in Fig. 6 for Au_{147} and $Au_{134}Fe_{13}$ (left) and for Au_{309} and $Au_{254}Fe_{55}$ (right). We notice that the stability of the cluster is not only maintained by replacing the inner gold core with iron, but that it actually slightly increases.

VI. VIBRATION SPECTRA AND SPECIFIC HEAT

In this section we present results related to the vibration dynamics of Au_{309} and $Au_{254}Fe_{55}$ clusters. First we obtain the vibrational eigenmodes by direct diagonalization of the dynamical matrix, and from this data we derive the vibration mode density of states $g(\nu)$ and the specific heat C_v. The latter was calculated using the formalism described by D'Agostino[35] and Maradudin.[36] Analytically,

$$\frac{C_v}{N} = \frac{k_B}{N}\sum_{i=1}^{N}\left[\frac{h\nu_i/2k_BT}{\sinh(h\nu_i/2k_BT)}\right]^2 = 3k_B\int_0^{\nu_{\max}} g(\nu)\left[\frac{h\nu/2k_BT}{\sinh(h\nu/2k_BT)}\right]^2 d\nu\,, \qquad (6)$$

where N is the number of modes (i.e., 927 in our case, including three uniform translations and three trivial rotations), and $\nu_{\max}$ is the largest value the frequency ν attains. In Figs. 7, 8, and 9 we display the vibration frequencies, the density of states, and phonon specific heat, respectively, for Au_{309} and $Au_{254}Fe_{55}$ clusters. The results for Au_{309} are quite similar to those obtained by previous authors.[35] The

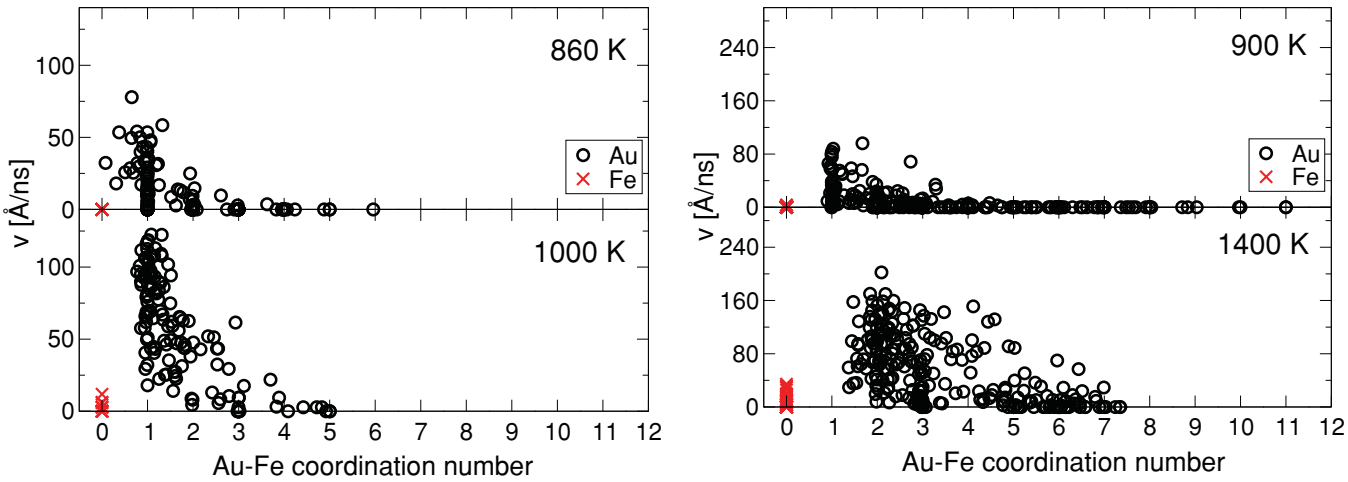

FIG. 5. (Color online) Atomic displacement speed versus average Au-Fe coordination for $Au_{134}Fe_{13}$ (left) and $Au_{254}Fe_{55}$ Au_{147} (right) clusters. The red × represent the Fe and the black open circles the Au atoms.

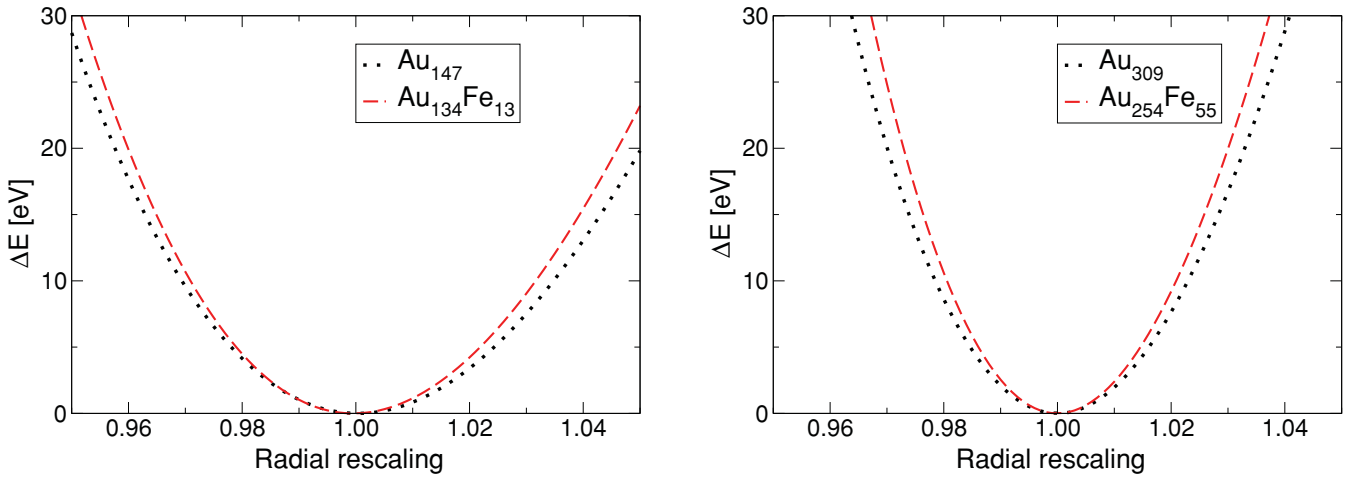

FIG. 6. (Color online) Hardness of Au_{147} and $Au_{134}Fe_{13}$ (left) and of Au_{309} and $Au_{254}Fe_{55}$ (right) clusters versus radial variation.

corresponding average potential energies per atom are $U = -3.94001$ eV/atom and $U = -4.00451$ eV/atom for Au_{309} and $Au_{254}Fe_{55}$, respectively.

It is well known that for a classical system the mechanically stable configuration corresponds to a minimum of the cohesive energy. However, quantum mechanical zero-point vibrations do not allow the atoms to remain motionless at their equilibrium positions in an energy eigenstate. Thus, at $T = 0$ there is a contribution to the energy given by

$$U_0 = \frac{1}{2}\sum_n h\nu_n\,, \tag{7}$$

which, in principle, can change the relative stability between different energy minima for the same cluster. Thus, U_0 is a relevant magnitude to evaluate. For Au_{309} and $Au_{254}Fe_{55}$ we obtained for these values 0.021 and 0.026 eV/atom, respectively.

The vibration eigenfrequencies ν for Au_{309} and $Au_{254}Fe_{55}$ are given in Fig. 7. We compute at zero temperature the frequencies for the thermally stabilized configurations; that is, we freeze the $T > 0$ configurations and calculate their normal modes. The (black) circles describe the $Au_{254}Fe_{55}$ structure during the heating process, starting from the same configuration already described and analyzed in the context of Fig. 1. After melting, the atomic arrangement changes and thus also the vibration spectrum $g(\nu)$, as illustrated by the (red) crosses in Fig. 7, which describe the cooling process. Finally, the (blue) triangles correspond to Au_{309}, both during heating and cooling, since the original cluster configuration is recovered after melting takes place. The vibration mode density of states $g(\nu)$ for Au_{309} and $Au_{254}Fe_{55}$ are given in Fig. 8 in the form of histograms. A slight decrease of the bandwidth for the pure gold cluster, as compared with the binary one, is observed, which is consistent with the vibration eigenfrequency spectrum of Fig. 7. However, a marked difference is observed in the form of $g(\nu)$ between the heating and cooling process [panels (a) and (b) of Fig. 8].

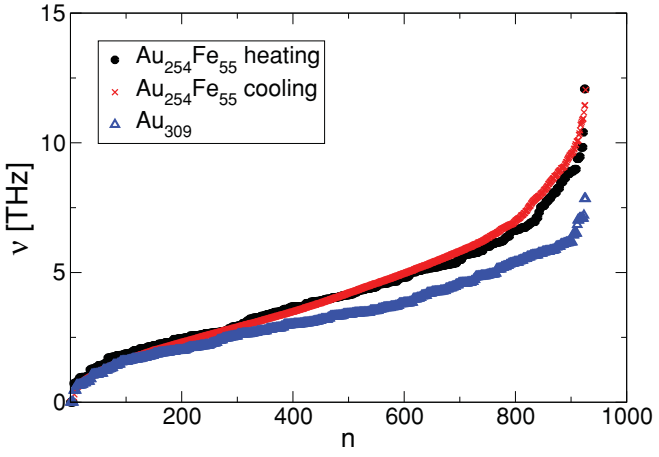

FIG. 7. (Color online) Vibration frequencies for Au_{309} (blue triangles); for $Au_{254}Fe_{55}$ (black circles) during the heating process; and for $Au_{254}Fe_{55}$ (red crosses) during the cooling process.

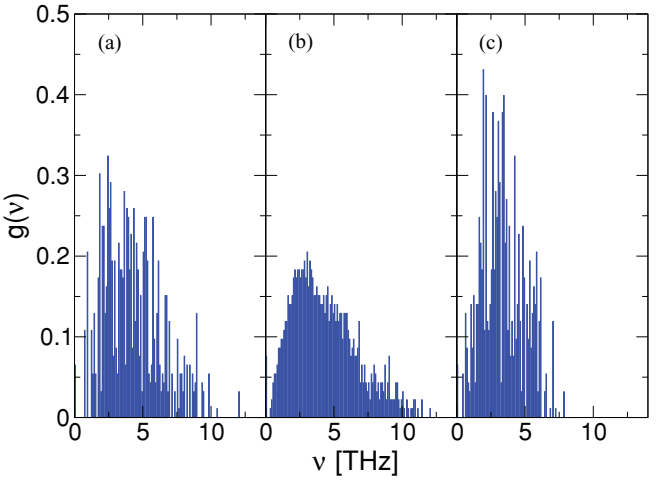

FIG. 8. (Color online) Vibration mode density of states histogram (a) for $Au_{254}Fe_{55}$ during the heating process; (b) after heating, during the cooling process for $Au_{254}Fe_{55}$; and (c) for Au_{309}.

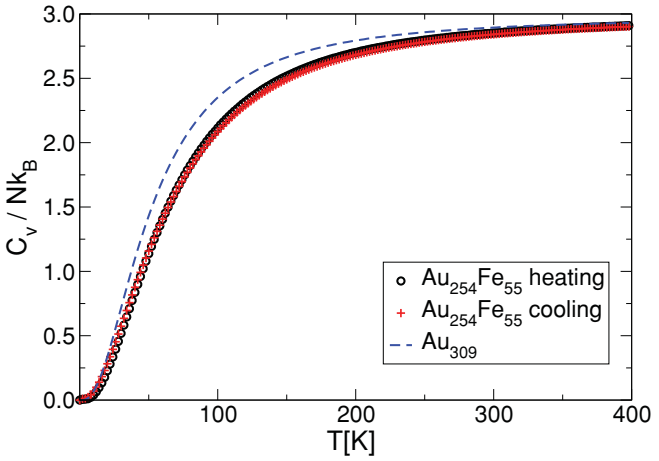

FIG. 9. (Color online) Specific heat of Au_{309} (blue dashes) and $Au_{254}Fe_{55}$ during heating (black circles) and cooling (red + symbols).

This difference is related to the disparate cluster configurations that result when cooling from the melt, but which do not reflect in the vibration eigenfrequencies of Fig. 7.

The specific heat of the $Au_{254}Fe_{55}$ and Au_{309} clusters is displayed in Fig. 9. Again the physics is consistent with Figs. 7 and 8, showing slightly larger values for the pure sample and little difference between the original structure and the one that develops after freezing.

As pointed out by Kara and Rahman,[37] at low temperatures the specific heat of nanoclusters deviates from the usual Debye $C_v \propto T^3$ low-temperature behavior of large systems, and displays a T^2 dependence instead. This important finding, which arises from the features in the vibrational density of states which are distinct from those of the bulk,[38] is also present in our results, as illustrated in Fig. 10, where we zoom in on the low-temperature ($T < 25$ K) tail of the specific heat. The largest deviation from linearity is observed for the heating of $Au_{254}Fe_{55}$, presumably due to the fact that it does not correspond to the lowest energy configuration of the nanocluster.

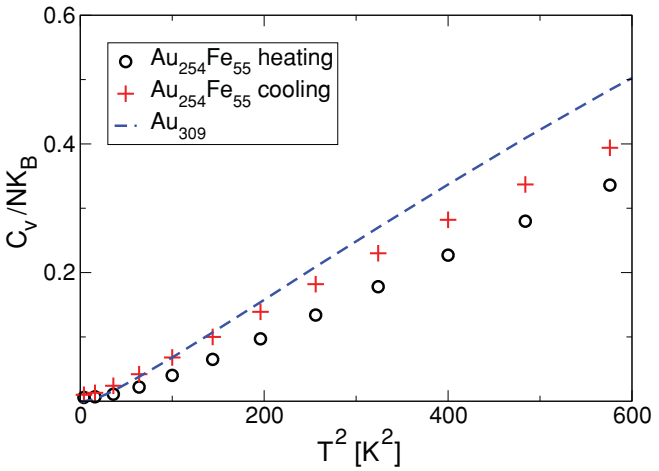

FIG. 10. (Color online) Low-temperature specific heat of Au_{309} (blue dashes) and $Au_{254}Fe_{55}$ during heating (black circles) and cooling (red + symbols) versus T^2.

VII. CONCLUSIONS

In this contribution we have studied gold nanoclusters, both with and without an iron core, by means of classical molecular dynamics (MD). Our main objectives were to calculate their properties, establish the stability of the system, and compare the characteristics of pure gold Au_N and binary $Au_{N-x}Fe_x$ nanoclusters. We focused our attention on four representative systems: Au_{147}, $Au_{134}Fe_{13}$, Au_{309}, and $Au_{254}Fe_{55}$, chosen because they correspond to magic number icosahedral structures, for both the gold and the iron.

The MD was carried out using modified[28] Finnis-Sinclair type potentials.[27] We evaluated the total energy as a function of temperature T, from 20 K up to well above the melting temperature, increasing T by 20 K steps during the simulations. The system was relaxed at every T step for 0.5 ns (i.e., half a million MD steps). On this basis we obtained the energy versus temperature behavior, data on the diffusion of the atoms, hardness, vibration eigenmodes, density of states, and specific heat of the system.

The melting process turned out to be quite different for the pure Au_N and binary $Au_{N-x}Fe_x$ nanoclusters. Pure gold melts at a significantly lower temperature than in the bulk, and has an associated hysteresis cycle, maintaining an icosahedral structure, as observed experimentally by Saha *et al.*[21] Binary clusters $Au_{N-x}Fe_x$ instead overcome a kinetic barrier[32] to settle into a lower energy configuration, which is maintained after freezing. Also the atomic diffusion process is quite different for pure and binary clusters. While pure gold clusters have a large diffusion coefficient above the solid-to-liquid transition, the iron of binary clusters has a much smaller atomic mean square displacement and never reaches the "surface" of the cluster. The hardness, defined as the variation of the total potential energy versus small changes of the distance of every atom to the center of mass of the cluster (radial rescaling), also suggests that binary clusters ($Au_{N-x}Fe_x$) are quite stable. In fact, the hardness of the nanoclusters with iron cores is slightly larger than that of pure gold clusters.

We also calculated the vibration spectrum, density of vibration eigenmodes, and specific heat. They show an energy increase for the eigenmodes, a widening of the bandwidth, and a decrease of the specific heat of the binaries relative to the pure gold clusters. All of our calculations are consistent with the stability of the $Au_{N-x}Fe_x$ nanocluster system.

ACKNOWLEDGMENTS

This work was supported by the Fondo Nacional de Investigaciones Científicas y Tecnológicas (FONDECYT, Chile) under Grants No. 1071062 and No. 1090225 (M.K.), No. 1080239 (G.G. and R.R.), and No. 1070854 (J.A.V.), the Financiamiento Basal para Centros Científicos y Tecnológicos de Excelencia, CEDENNA (G.G., M.K., R.R., and J.A.V.), and DOE Grant No. DE-FG02-07ER46354 (T.S.R.).

[1]M. Faraday, Philos. Trans. R. Soc. London**147**, 145 (1857).
[2]P. Buffat and J.-P. Borel, Phys. Rev. A **13**, 2287 (1976).
[3]M. Haruta, Catalysis Today **36**, 153 (1997).
[4]A. Sanchez, S. Abbet, U. Heiz, W. D. Schneider, H. Häkkinen, and U. Landman, J. Phys. Chem. A **103**, 9573 (1999).
[5]M. Valden, X. Lai, and D. W. Goodman, Science **281**, 1647 (1998).
[6]C. Binns, Surf. Sci. Rep. **44**, 1 (2001).
[7]H. Häkkinen, M. Moseler, O. Kostko, N. Morgner, M. A. Hoffmann, and B. v. Issendorff, Phys. Rev. Lett. **93**, 093401 (2004).
[8]I. M. L. Billas, A. Chatelain, and W. A. de Heer, Science **265**, 1682 (1994).
[9]W. L. Barnes, A. Dereux, and T. W. Ebbesen, Nature (London) **424**, 824 (2003).
[10]B. Gilbert, F. Huang, H. Zhang, G. A. Waychunas, and J. F. Banfield, Science **305**, 651 (2004).
[11]T. VanHoof and M. Hou, Phys. Rev. B **72**, 115434 (2005).
[12]Z. Kuntova, G. Rossi, and R. Ferrando, Phys. Rev. B **77**, 205431 (2008).
[13]D. H. Kim, H. Y. Kim, J. H. Ryu, and H. M. Lee, PhysChemChemPhys **11**, 5079 (2009).
[14]T. L. G. Li, X. Lü, Q. Wang, K. Wang, and J. He, Phys. Lett. A **374**, 1769 (2010).
[15]R. Ferrando, J. Jellinek, and R. L. Johnsoton, Chem. Rev. **108**, 845 (2008).
[16]Y. P. Lee, Y. V. Kudryavtsev, V. V. Nemoshkalenko, R. Gontarz, and J. Y. Rhee, Phys. Rev. B **67**, 104424 (2003).
[17]K. Takanashi, S. Mitani, M. Sano, H. Fujimori, H. Nakajima, and A. Osawa, Appl. Phys. Lett. **67**, 1016 (1995).
[18]K. Takanashi, S. Mitani, K. Himi, and H. Fujimori, Appl. Phys. Lett. **72**, 737 (1998).
[19]A. Naitabdi and B. Roldan-Cuenya, Appl. Phys. Lett. **91**, 113110 (2007).
[20]B. Roldan-Cuenya, L. K. Ono, J. R. Croy, A. Naitabdi, H. Heinrich, J. Zhao, E. E. Alp, W. Sturhahn, and W. Keune, Appl. Phys. Lett. **95**, 143103 (2009).
[21]D. K. Saha, K. Koga, and H. Takeo, Eur. Phys. J. D **9**, 539 (1999).
[22]T. Massalki, H. Okamoto, and P. R. Subramanian, *Binary Alloy Phase Diagrams*, 2nd ed. (ASM International, Metals Park, OH, 1990).
[23]P. M. Paulus, H. B. Bönnemann, A. M. van der Kraan, F. Luis, J. Sinzig, and L. J. de Jongh, Eur. Phys. J. D **9**, 501 (1999).
[24]W. L. Zhou, E. E. Carpenter, J. Lin, A. Kumbhar, J. Sims, and C. J. O'Connor, Eur. Phys. J. D **16**, 289 (2001).
[25]F. Ercolessi, [http://www.fisica.uniud.it/∼ercolessi/md/f90/].
[26]F. Ercolessi, M. Parinello, and E. Tosatti, Philos. Mag. A **58**, 213 (1988).
[27]M. W. Finnis and J. E. Sinclair, Philos. Mag. A **45**, 5056 (1984).
[28]X. D. Dai, Y. Kong, J. H. Li, and B. X. Liu, J. Phys. Condens. Matter **18**, 4527 (2006).
[29]G. Kresse and J. Hafner, Phys. Rev. B **47**, 558 (1993).
[30]G. Kresse and J. Furthmüller, Comput. Mater. Sci. **6**, 15 (1996).
[31]G. Kresse and J. Furthmüller, Phys. Rev. B **54**, 11169 (1996).
[32]C. Mottet and J. Goniakowski, Surf. Sci. **566-568**, 443 (2004).
[33]M. Schmidt, R. Kusche, W. Kronmüller, B. von Issendorff, and H. Haberland, Phys. Rev. Lett. **79**, 99 (1997).
[34]M. Schmidt, R. Kusche, W. Kronmüller, B. von Issendorff, and H. Haberland, Nature (London) **393**, 238 (1998).
[35]G. D'Agostino, Philos. Mag. B **76**, 433 (1997).
[36]A. Maradudin, editor, *Theory of Lattice Dynamics in the Harmonic Approximation*, Solid State Physics, Suppl. 3 (Academic Press, New York, 1971).
[37]A. Kara and T. S. Rahman, Surf. Sci. Rep. **159**, 56 (2005).
[38]A. Kara and T. S. Rahman, Phys. Rev. Lett. **81**, 1453 (1998).